SF2A 2006
D. Barret, F. Casoli, T. Contini, G. Lagache, A. Lecavelier, and L. Pagani (eds)

NUMERICAL SIMULATION OF MRI: TOWARDS A SYSTEMATIC CHARACTERIZATION OF TURBULENT TRANSPORT IN ACCRETION DISKS.

G. Lesur[1] and P.-Y. Longaretti[1]

Abstract. From the early 90s, the magneto rotational instability has found to be the most promising instability to explain turbulent transport in accretion disks. However, some important issues have been overlooked in previous studies and need to be studied to quantify the role of MRI-driven turbulence in disks. We present here a numerical study using a pseudo spectral incompressible 3D code, with explicit viscosity and resistivity. First, we show that close to the marginal stability limit, the turbulent transport is unexpectedly large, and highly time-dependent. Second, we exhibit a substantial dependance of the global transport on the magnetic Prandtl number, which may have an important role in many astrophysical objects such as YSO accretion disks (Pr=10^{-8}). More generally, these results exhibit the need to control the dissipation process in astrophysical simulations.

1 Introduction

Transport in accretion disks has always been a central problem in the disk community. The first α model (Shakura & Sunyaev 1973) already assumed a strong turbulence, leading to an effective viscosity orders of magnitude higher than molecular viscosity. However, the physical origin of the turbulence in disks is still highly debated. Since unstratified keplerian flows are known to be linearly stable to small perturbation, a first idea was to test an hypothetical nonlinear instability which can trigger turbulence with finite amplitude perturbations. This question was studied both experimentally (Richard & Zahn 1999) and numerically (Balbus et al. 1996; Hawley et al. 1999) but recent results showed that the transport due to this instability would be far too low to explain observations (Lesur & Longaretti 2005).

An MHD instability in accretion disks was found by Balbus & Hawley (1991), the magnetorotational instability (MRI). This instability has been extensively studied since then, mainly with local unstratified (Hawley et al. 1995) and stratified (Stone et al. 1996) 3D simulations, and global (Hawley 2000) disk simulations. However, the dissipation of turbulent fields in these simulations is not controlled : no physical term is introduced to take care of viscosity and resistivity. One may wonder whether the numerical dissipation introduced by these simulation had an impact on the statistical quantities useful for disks models, such as transport coefficients.

This issue is adressed here, using a 3D spectral Fourier code, with a full control over viscosity, resistivity and numerical dissipation. First, we present the MHD equation set in the shearing box frame (Hawley et al. 1995), and we exhibit the dispersion relation, including viscosity and resistivity. Then, we present new results on the behaviour of the MRI when computed near the threshold of the instability. The role of magnetic Prandtl number, which may have important consequences on YSO disks physics, will be discussed in the third part of this work. Last, a brief discussion is provided, exhibiting numerical artifacts that may influence our results.

2 Linear instability analysis

The MRI has already been studied extensively analytically by Balbus & Hawley in 1991. However, to take care of dissipation, one needs to add the viscous and resistivity terms to the basis equations. A full calculation of this instability, including viscous and resistive effects will be detailed in Lesur & Longaretti (2007).

[1] Laboratoire d'Astrophysique - Observatoire de Grenoble BP 53, 38041 GRENOBLE CEDEX 9

We define the shear $S = -r\partial_r\Omega$, where Ω is the rotation rate in the local frame ($S = 3/2\Omega$ for Keplerian rotation profile). We concider only axisymmetic perturbations for simplicity, and assume $Pr = \nu/\eta = 1$ for definiteness, where ν is the kinematic viscosity, η the resistivity and Pr the magnetic Prandtl number. Note that this non-dimensional number achieves very large variations from one type of disk to another (down to 10^{-8} in protoplanetary disks and up 10^4 in AGNs, although such estimates are highly uncertain). In our simulations, it is restricted to the $\sim 10^{-1}$ to ~ 10 range, due to numerical constraints. Defining the epicyclic frequency $\kappa^2 = 2\Omega(2\Omega - S)$ and the Alfvén speed $v_a^2 = B_0^2/\mu_0\rho$ where B_0 is the mean vertical magnetic field, one gets the following condition for the instability of a k_z mode:

$$\nu^2 < \frac{\sqrt{\kappa^4 + 16k_z^2 v_a^2 \Omega^2}}{2k_z^4} - \frac{v_a^2}{k_z^2} - \frac{\kappa^2}{2k_z^4} \qquad \text{INSTABILITY} \tag{2.1}$$

One can check that the higher ν values are found for $k_z = min(k_z) = 2\pi/H$, which correspond to the typical z channel solutions. Defining the Reynolds number as $Re = SH^2/\nu$ where H is the numerical box height or the typical disk height, and using the plasma parameter [1] $\beta = v_a^2/S^2H^2$, we plot the instability curve on fig. 1.

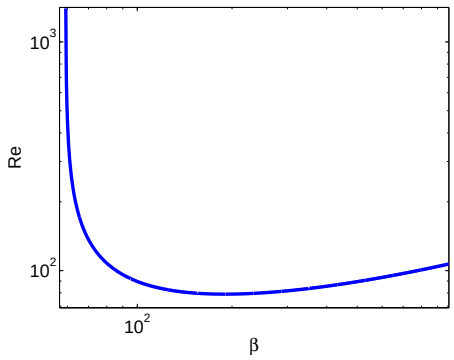

Fig. 1. MRI linear stability limit

Note that the instability has 2 different behaviors, depending on the β parameter:

- High β regime , corresponding to a low magnetic pressure. In this regime, one finds a nearly constant critical Reynolds ($Re_c \simeq 80$), which corresponds to a standard behavior in fluid dynamics: the growth time scale of the most instable mode must be lower than the dissipation time scale, defined by $\tau_d \simeq k^2/\nu$.
- Low β regime, which is nearly Reynolds independent. In this region, one can define a critical β ($\beta_c = 59$) for which the MRI is lost. This behavior can be explained considering the smallest instable mode : as β goes to lower values, the smallest instable mode gets larger (see eq. 2.1). At one point this smallest mode gets larger than the scale height H and the instability is lost. Since this phenomenon takes place at large scale, the Reynolds number has naturally no role to play in it. Note that this regime is not specific to our unstratified calculation, since similar results are found for stratified medium with $\beta_c \simeq 1$ (see Gammie & Balbus 1994).

3 Numerical Results

3.1 Numerical code

The code used for these simulations is an MHD extension of the HD code used in Lesur & Longaretti (2005), and extensively described in there. This code is a full 3D, spectral (Fourier), MPI, incompressible code, using the FFTW libraries for FFTs. All the simulations presented hereafter are done using $128 \times 64 \times 64$ xyz resolution with box dimensions $4 \times 1 \times 1$. (x being the azimutal direction and y the radial direction).

[1] This definition differs from the standard one by factors of order unity when the constraint of vertical hydrostatic equilibrium holds.

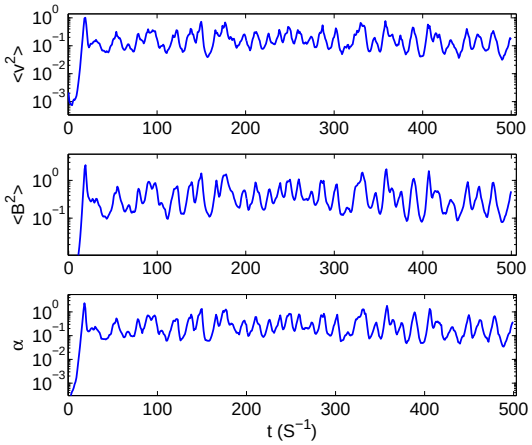

Fig. 2. $\beta = 200$, Re=3200 run

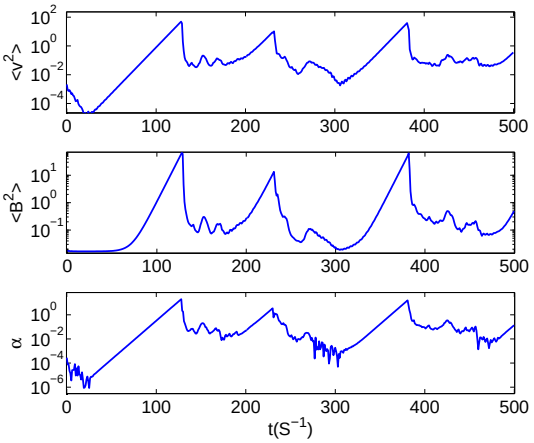

Fig. 3. $\beta = 60$, Re=3200 run

3.2 MRI Behaviour near the low β instability threshold

We present here two simulations, a classical one made at $\beta = 200$ and $Re = 1600$ (run 1) and a simulation made near the β treshold for $\beta = 60$ and $Re = 3200$ on figs (2) and (3). One immediately notes a strong difference between these two simulation. On run 1, we find a classical MRI behaviour, as studied by Hawley et al. (1995), caracterised by $\alpha \sim 10^{-1}$ and random variations in all the statistical quantities. However, run 2 exhibits strong exponential growth ("bursts") for about 100 shear times (∼10 orbits), and a sudden fall of the turbulent motions. This behavior is explained as follows : for such low β only the largest wavelength mode is unstable (and not smaller scales), which is then allowed to grow for many shear times, as this mode is an exact nonlinear solution to the incompressible equations of motions (Goodman & Xu 1994). We therefore observe the growth of the channel flow as seen by Hawley & Balbus (1992). However, as this channel solution gets stronger, secondary instabilities such as Kelvin Helmoltz instability destroys the channel solution quickly and a new cycle starts (see Goodman & Xu 1994 for a detailed description of these secondary instabilities). Note that due to this phenomenon, one cannot consider α as a constant during time and new time dependant transport models are needed for low β disks. Moreover, one can reach very high transport values ($\alpha \simeq 5$), leading to the question of the role of compressibility in such simulations.

3.3 Magnetic Prandtl effect on transport coefficients

Since all the previously published simulations were performed without any control on the dissipation scales, one may wonder if these smallest scales have an impact on large scales and therefore transport coefficients. This issue is studied here varying the Prandtl number defined in section 2. This parameter allows us to change the dissipation scale of the velocity and magnetic fields. However, one cannot go far from $Pr = 1$ numerically, since one wants to resolve both the velocity and magnetic dissipations scales. We present on figure 4 the result of such simulations: we plot the mean transport coefficient (α) as a function of the Prandtl number, for various Reynolds numbers (note that the Reynolds number quantify the viscous disspation). Statistics are done using 500 shear times, removing the first 100 shear times to let the transition period from the initial state decay. From these plots, one find a strong correlation between the Prandtl number and the transport coefficient so that $\alpha \propto Pr^{0.25-0.5}$.

Finally, this effect may be explained by a retroaction of the magnetic field small scales which enhance the transport on large scales. However, this new effect needs to be studied with other codes/resolutions to get a general and predictive description. This kind of description is required since one may wonder about the transport coefficient value for Prandtl number as low as 10^{-8} such as in protoplanetary disks, which cannot be reached numerically.

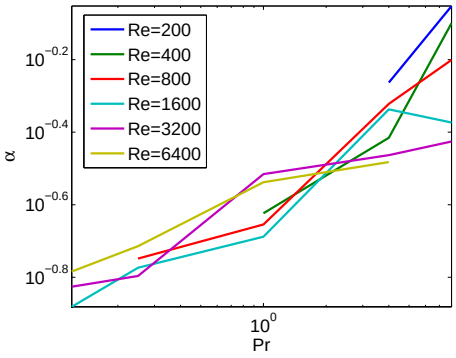

Fig. 4. Prandtl effect

4 Discussion

In the previous section, we exhibited a new behavior of the MRI near the low β instability threshold. This phenomenon is shown for simulations with $\beta = 60$, i.e near the threshold in our simulation box. In vertically stratified disks, such threshold is obtained for the same physical reasons, but for $\beta \sim 1$ (Gammie & Balbus 1994). The use of periodic boundary conditions (vertical) or semi periodic (radial) boundary conditions may enhance the role of the channel flow solution and real disk solutions may break up sooner than observed in our local simulations, leading to smaller bursts. Moreover, $\alpha > 1$ leads to supersonic motions and compressible numerical simulations are needed for this kind of phenomenon, which may exhibit new secondary compressible instabilities. All these issues leads to the conclusion that low β MRI should lead to weaker bursts and therefore smaller transport coefficient than observed in our simulations. However, there is no physical reason why the turbulence bursts would be suppressed, and we believe that these bursts may be a strong signature of $\beta \sim 1$ stratified disks where MRI-driven turbulence is present.

The other new result shown in this paper is a correlation between the transport efficiency, and the magnetic Prandtl number, leading to a higher transport coefficient for larger Prandtl numbers. As previously, one should question the role of the boundary conditions used in these simulations. However, the possible biases are less obvious and tests with plane radial walls need to be performed to get a grasp on boundary condition effects. Moreover, one needs to check the correlation at higher resolutions, and if possible higher Prandtl numbers, using different kind of codes to get a better characterization and a physical description of the phenomena involved in this observation.

The simulations presented in this paper has been performed both at IDRIS (French national computational center) and at the SCCI (Grenoble Observatory computational center)

References

Balbus, S.A., & Hawley, J.F. 1991, ApJ, 376, 214
Balbus, S.A., Hawley, J.F., & Stone, J.M. 1996, ApJ, 467, 76
Gammie, F.G., & Balbus, S.A. 1994, MNRAS, 270, 138
Goodman, J., & Xu, G. 1994, ApJ, 432, 213
Hawley, J.F. 2000, ApJ, 528, 462
Hawley, J.F., & Balbus, S.A. 1992, ApJ, 400, 595
Hawley, J.F., Balbus, S.A., & Winters, W.F. 1999, ApJ, 518, 394
Hawley, J.F., Gammie, C. F., & Balbus, S.A. 1995, ApJ, 440, 742
Lesur, G., & Longaretti, P-Y. 2005, A&A, 444, 25
Lesur, G., & Longaretti, P-Y. 2007 *in prep.*
Richard, D., & Zahn, J-P. 1999, A&A, 347, 734
Shakura, N.I., & Sunyaev, S.A. 1973, A&A, 24, 337
Stone, J.M., Hawley, J.F., Gammie, C.F., & Balbus, S.A. 1996, ApJ, 463, 656